Nearest Neighbor Classification of Binary Channel States for Secure Human Body Communication

Ai-ichiro Sasaki, *Member, IEEE*, and Akinori Ban

***Abstract*— Human body communication (HBC) is a short-range communication technique in which the human body is used as a data transmission channel. Although the HBC was originally proposed for connecting multiple mobile devices, it is also useful for quickly linking mobile and fixed devices. The latter feature can be applied to smart identification of persons. The HBC channel is formed by a capacitive coupling among the body, mobile and fixed devices, and earth. Consequently, if an outsider approaches the HBC system, that person inevitably becomes involved in the system because of the capacitive coupling. In this situation, a mobile device of the outsider accidentally transmits data signals and misidentification occurs. This is a serious problem in terms of communication system security. An effective approach for resolving this problem is to predict whether the outsider is involved in the HBC system based on signal information received by the fixed device. In this article, we present a method for correctly predicting the existence of the outsider involved in the HBC system based on channel gain features detected by the fixed device. As the problem can be viewed as a binary classification problem, we adopted k-nearest neighbor method (k-NN), which is a supervised machine learning algorithm, for solving it. A key to correctly execute and evaluate k-NN is to obtain the reliable channel gain data for training and evaluation. We utilized optical devices for correctly measuring the HBC channel gain and acquired 360 samples of the channel gain data. It was demonstrated that error-free classification was possible with the k-NN classifier for the 360 samples. We obtained three key findings for reducing classification errors. First, $k = 1$ is best for the k-NN classifiers. Second, 1-norm is better than 2-norm for calculating error functions of k-NN classifiers. Third, the preprocessing that includes partition and normalization of channel gain data is highly effective.**

***Index Terms*— Communication channels, communication system security, identification of persons, machine learning, nearest neighbor methods.**

I. Introduction

THE concept of human body communication (HBC) was proposed by Zimmerman [1] in 1996. The basic idea was to use the human body as data transmission channel for linking multiple wearable devices attached to the user's body. This novel idea has received attention, especially in the community of human-interface researchers [2], [3], [4]. However, research on HBC was not widespread because wearable devices were not popular at that time. Furthermore, the signal transmission mechanism of the HBC channels was not well understood.

At the beginning of the 21st century, Nippon Telegraph and Telephone Corporation (NTT) began full-scale research on HBC [5], [6], [7], [8], [9]. However, the target application of NTT was communication between fixed and mobile devices rather than that among wearable devices. During this period, one of the main applications of HBC technologies was the smart identification of persons, and several other Japanese companies attempted to commercialize the technologies. Several studies have been conducted to understand the signal transmission mechanism in HBC channels. It has become possible to understand the mechanism of HBC after the proposal of equivalent circuit models of HBC channels [10], [11], [12], [13], [14], [15].

However, two major problems exist from a practical perspective. One of these problems is the difficulty in obtaining the required signal-to-noise ratio (SNR) for stable communication. The main factor in SNR reduction is environmental noise. Subsequently, a method for reducing noise was proposed [16], [17]. Owing to these methods, it has become possible to obtain a reasonable SNR.

The other problem is that accidental data transmission can occur in personal identification systems that use HBC technologies. The essential principle of HBC is that data are carried by the electric fields generated around the human body. Because of this principle, the electric fields existing around a person in an HBC system are easily transmitted to nearby outsiders. Therefore, if an outsider with a mobile device unintentionally approaches HBC systems, his device may accidentally transmit data signals to a fixed device via the person, and undesired identification processes are triggered. This is a serious problem in terms of the security of communication systems. However, this serious problem has not been openly discussed in the academic community.

Subsequently, the upsurge in HBC research has ended in Japan. However, HBC technologies have been investigated continuously outside Japan [18], [19], [20], [21], [22], [23], [24], [25], [26], [27], [28], [29], [30], [31], [32], [33], [34], [35]. Recently, wearable devices and the "Internet of Things" (IoT) have become popular [36]. This situation also supports the validity of Zimmerman's original concept, and widespread research on HBC technologies has resumed. However, the second serious problem is yet to be investigated.

Consequently, we have been studying methods to address the second problem [37], [38]. Because the physical states of

Manuscript received 1 June 2022; revised 16 August 2022; accepted 11 September 2022. Date of publication 26 September 2022; date of current version 14 October 2022. The Associate Editor coordinating the review process was Dr. Huang-Chen Lee. *(Corresponding author: Ai-ichiro Sasaki.)*

The authors are with the Department of Electronic Engineering and Computer Science, Kindai University, Higashi-Hiroshima, Hiroshima 739-2116, Japan (e-mail: aisasaki@hiro.kindai.ac.jp; 2133850038t@hiro.kindai.ac.jp).

Digital Object Identifier 10.1109/TIM.2022.3209796

the HBC channels change when an outsider approaches the HBC system, the frequency dependence of the channel gain $G(f)$ inevitably changes as well. This implies the possibility of predicting whether the outsider is involved in the HBC system based on $G(f)$, which can be calculated from the signals received by the fixed device. If we can predict the existence of an outsider involved in the HBC system, the second serious problem may be resolved by system-level measures.

Based on this strategy, we attempted to predict the existence of an outsider from the measured $G(f)$ [37], [38]. The problem of predicting whether an outsider is involved in the HBC system can be viewed as a binary classification problem. We adopted a machine learning approach to solve the classification problem. Our preliminary studies have shown that this strategy is feasible and that machine learning is effective for prediction. However, in previous studies, the prediction error could not be reduced to less than 10%. Furthermore, only outlines of our studies are briefly reported in [37] and [38].

In this article, we detail our studies for detecting outsiders included in HBC systems. The original features of this study are as follows: First, we calculated $G(f)$ from the equivalent circuit models of the HBC systems and compared them with the measured results. It was shown that although $G(f)$ measured without the outsider coincided well with the circuit model, $G(f)$ measured with the outsider did not agree with the model. Second, we adopted the k-nearest neighbor (k-NN) method as the machine learning algorithm and analyzed the performance of k-NN in detail. Third, we proposed an appropriate procedure for preprocessing the training data to predict the existence of the outsider. Fourth, we found the best parameters for executing k-NN and accomplished an error-free prediction of the existence of the outsider by adopting the parameters and preprocessing.

In Section II, HBC channel models, with and without the outsider, are introduced and $G(f)$ is calculated from the models. The calculated results were compared with the typical measurement results. In Section III, the details of $G(f)$ are explained. In addition, the experimental system, conditions, and results were described in detail in this section. In Section IV, the performance of k-NN classifiers is thoroughly investigated and the preprocessing procedure is described. It is revealed that the 1-norm is better than the 2-norm for calculating error functions. Furthermore, we can see that the best classifier is the 1-NN classifier, that is $k = 1$.

II. Channel Models of HBC Systems

A. Signal Transmission Models of HBC Channels

The basic concept of HBC is illustrated in Fig. 1. In this study, we focus on the uplink channel, where data are sent from a mobile transmitter (M-TX) to a fixed receiver (F-RX). A pair of mobile electrodes M+ and M− are connected to M-TX. Similarly, a pair of fixed electrodes F+ and F− are connected to F-RX. The downlink channel can be understood in a similar manner [37].

Data signals generated by M-TX are applied between M+ and M−. The human body can be regarded as a conductor covered by insulators such as skin, clothes, and shoes.

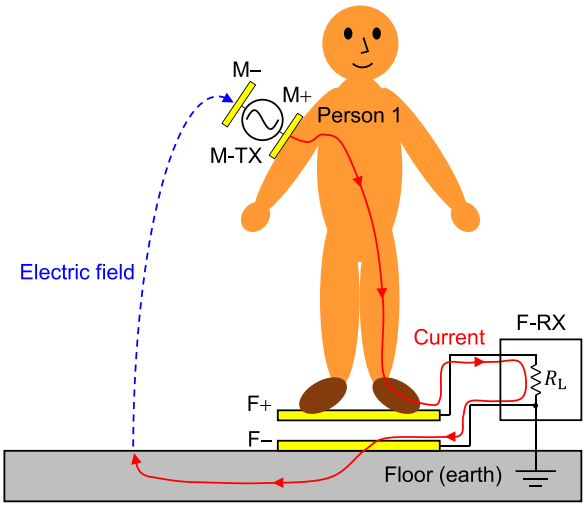

Fig. 1. Conceptual image of an HBC uplink channel in an ordinary state.

Therefore, when Person 1 possessing M-TX rides on F+, signal currents are delivered from M-TX to F-RX via their body. The conduction currents flowing inside F-RX induce voltages between F+ and F−. Consequently, it becomes possible to receive data sent from M-TX by detecting the induced voltages. Because the F-RX is driven by an ac power cord, F− and ground (GND) of F-RX are inevitably earthed. On the other hand, the M− electrode and GND of M-TX are electrically isolated from the earth because the M-TX is driven by a battery. In other words, the M− and GND of M-TX are always floating. The floating nature of M− is essential for understanding the characteristics of HBC channels.

As shown in Fig. 1, M− is capacitively coupled to a floor, which is regarded as earth. In other words, M− and earth form a capacitor. Therefore, when voltages are applied between M+ and M−, electric fields (displacement currents) shown by the dashed curve in Fig. 1 are generated between M− and the floor. Finally, the HBC channel is formed by a closed loop composed of conduction currents (solid red curve) and displacement currents (dashed blue curve). As shown in Fig. 3, the HBC channel can be modeled by an equivalent circuit, which is explained in Section II-B. We call the channel state represented in Fig. 1 the "ordinary state."

A conceptual image of an undesirable situation, where an outsider exists in the vicinity of F+, is depicted in Fig. 2. In this situation, Person 1 without M-TX stands on F+, and an outsider equipped with M-TX exists in the vicinity of Person 1. If Person 1 were absent, the electric fields generated between M− and F+ would be extremely weak. Therefore, the signals sent from M-TX will not be delivered to F-RX. This situation is correct because the outsider is not standing on F+. However, when Person 1 is on F+, the signals transmitted from M-TX of the outsider are delivered via Person 1 to F-RX because the capacitance between M− and Person 1 increases considerably. This situation is undesirable because signals generated from an outsider who is not standing on F+ are accidentally delivered to F-RX. It should be emphasized that signals sent from a person who is not on F+ must not be delivered to F-RX.

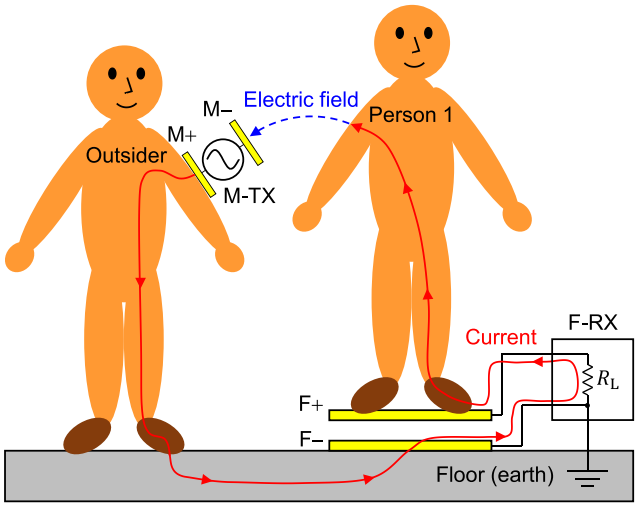

Fig. 2. Conceptual image of an HBC uplink channel in an extraordinary state.

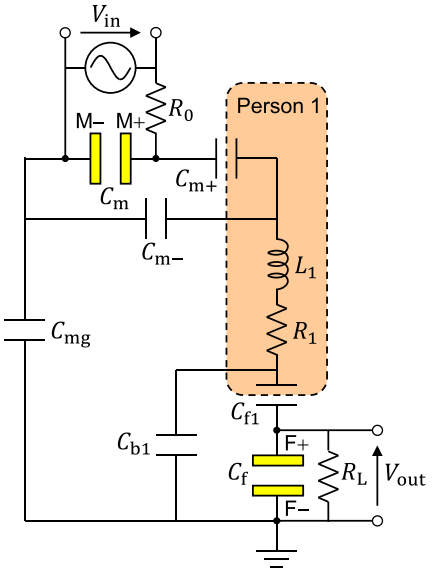

Fig. 3. Equivalent circuit model of an HBC uplink channel in an ordinary state.

We call the problematic channel state shown in Fig. 2 the "extraordinary state."

Although the occurrence of an extraordinary state is a serious concern from the point of view of communication system security, it appears difficult to completely prevent its occurrence. A reasonable approach to address this problem is to predict the occurrence of the extraordinary state. This is due to the fact that if we can predict the occurrence of an extraordinary state, security problems may be resolved by system-level measures. As shown in Figs. 1 and 2, the HBC channels of the two states are physically different. Because the frequency dependence of the channel gain $G(f)$ is inevitably affected by the physical state of the HBC channels, it is possible to predict whether the current channel state is ordinary or extraordinary based on $G(f)$ measured by F-RX. This problem can be viewed as a binary classification of measured

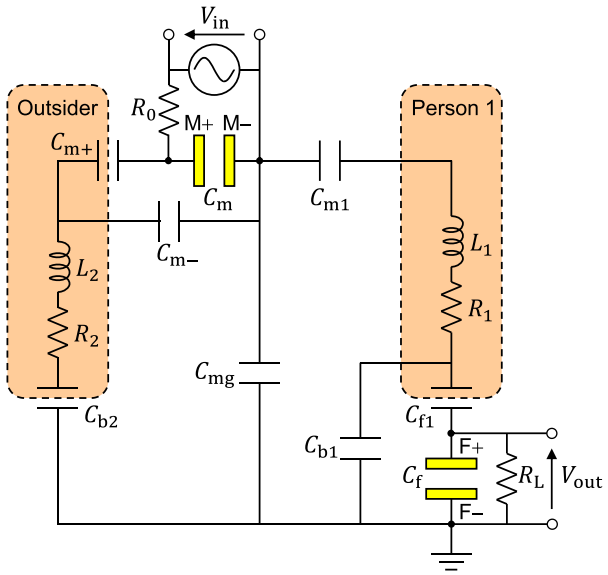

Fig. 4. Equivalent circuit model of an HBC uplink channel in an extraordinary state.

$G(f)$ into ordinary or extraordinary states. The details of the channel gain characteristics are discussed in Section II-B.

B. Analysis of Channel Models

There are two major schemes for establishing HBC systems [13], [15], [22], [26], [31]: capacitive [1], [10], [14], [16], [19] and galvanic coupling schemes [11], [29], [30]. In this study, we consider HBC systems that adopt a capacitive coupling scheme. The conceptual images shown in Figs. 1 and 2 represent the capacitive coupling scheme, where only one mobile electrode (M+) faces the human body. An advantage of this scheme is that a relatively large channel gain can be obtained. However, as shown in Fig. 2, a problematic extraordinary state is often induced. Conversely, for the galvanic coupling scheme, the channel gain becomes considerably small in comparison with that obtained with the capacitive coupling scheme [31]. Therefore, only short-range applications are available with the galvanic coupling scheme. Because the signals transmitted from the outsider are rapidly attenuated by the galvanic coupling scheme, the extraordinary state is not caused by this scheme.

In this study, we analyzed the frequency dependence of the HBC channel gain obtained using the capacitive coupling scheme. The HBC channels for this scheme can be reasonably described by circuit models [1], [10], [12], [16], [17]. Therefore, we also used circuit models to analyze the HBC channel characteristics.

The HBC channel models adopted for ordinary and extraordinary states are shown in Figs. 3 and 4, respectively. As mentioned previously, our focus was on uplink channels. In Figs. 3 and 4, the M-TX is described as a voltage source that applies the signal voltage V_{in} between mobile electrodes M+ and M−. F-RX is described as a pair of electrodes F+ and F−. When V_{in} is applied between M+ and M−, the received signal voltage V_{out} is induced between F+ and F−. The electric

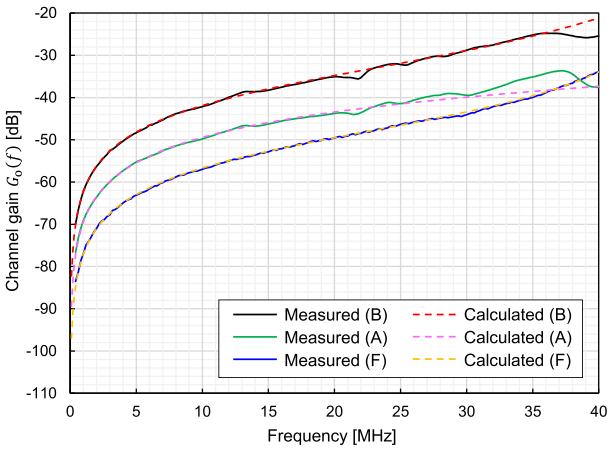

Fig. 5. Typical channel gain features of an ordinary state.

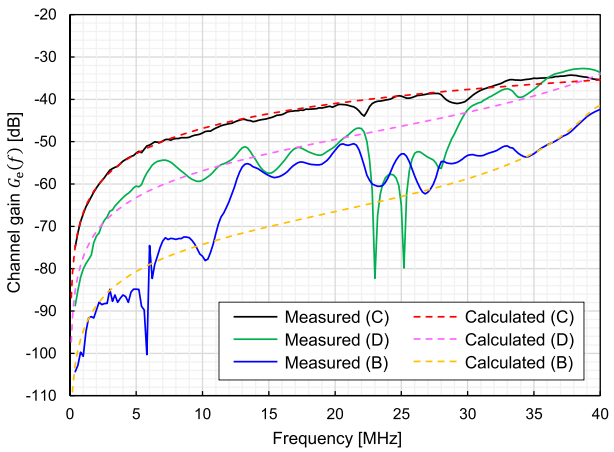

Fig. 6. Typical channel gain features of an extraordinary state.

TABLE I
PARAMETERS USED FOR PLOTTING CHANNEL GAIN FEATURES IN FIGS. 5 AND 6

Ordinary state (Fig. 5)		
Parameters	Values	Conditions
R_0	50 [Ω]	B, A, F
R_1	150 [Ω]	B, A, F
R_L	50 [Ω]	B, A, F
C_{b1}	20 [pF]	B, A, F
C_f	30 [pF]	B, A, F
C_{f1}	71 [pF]	B, A, F
C_m	5.4 [pF]	B, A, F
C_{m+}	7.1 [pF]	B, A, F
C_{m-}	1.0 [pF]	B, A, F
C_{mg}	7.0 [pF]	B
	2.0 [pF]	A
	0.72 [pF]	F
L_1	3.4 [μH]	B
	1.5 [μH]	A
	18.4 [μH]	F

Extraordinary state (Fig. 6)		
Parameters	Values	Conditions
R_0	50 [Ω]	C, D, B
R_1	150 [Ω]	C, D, B
R_2	150 [Ω]	C, D, B
R_L	50 [Ω]	C, D, B
C_{b1}	20 [pF]	C, D, B
C_{b2}	71 [pF]	C, D, B
C_f	30 [pF]	C, D, B
C_{f1}	71 [pF]	C, D, B
C_m	5.4 [pF]	C, D, B
C_{m+}	7.1 [pF]	C, D, B
C_{m-}	1.0 [pF]	C, D, B
C_{mg}	2.0 [pF]	C, D, B
C_{m1}	4.0 [pF]	C
	0.9 [pF]	D
	0.11 [pF]	B
L_1, L_2	0.3 [μH]	C
	5.0 [μH]	D
	9.5 [μH]	B

fields generated around the HBC system are represented as capacitors in Figs. 3 and 4.

We define HBC channel gain by the following equation:

$$G(f)\ [\mathrm{dB}] \triangleq 20\log_{10}\left|\frac{V_{\mathrm{out}}(f)}{V_{\mathrm{in}}(f)}\right|. \tag{1}$$

As shown in Figs. 3 and 4, the HBC channel gains for both states depend on several parameters. The HBC channel gains can be formally written as

$$G_o(f) = G_o(f; L_1, R_0, R_1, R_L, C_{b1}, C_f, C_{f1}, C_m, C_{m+}, C_{m-}, C_{mg}) \tag{2}$$

$$G_e(f) = G_e(f; L_1, L_2, R_0, R_1, R_2, R_L, C_{b1}, C_{b2}, C_f, C_{f1}, C_m, C_{m1}, C_{m+}, C_{m-}, C_{mg}) \tag{3}$$

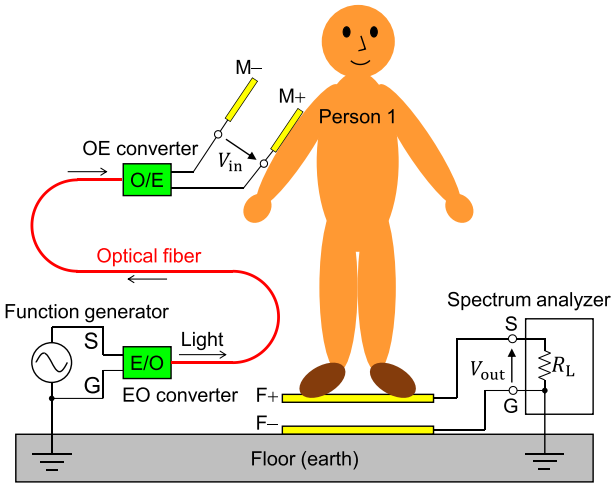

Fig. 7. Setup for evaluating HBC uplink channel gain by using EO/OE converters in an ordinary state.

where G_o and G_e represent the channel gains of ordinary and extraordinary states, respectively. The explicit forms of $G_o(f)$ and $G_e(f)$ can be obtained by analyzing the circuit models shown in Figs. 3 and 4, respectively; however, we omit writing them down because their explicit forms are very long.

Three typical examples of the measured $G_o(f)$ are shown by solid curves in Fig. 5. The black and green curves were obtained when the M-TX, a pair of mobile electrodes (M+ and M−), was put in the user's pant and shirt pockets, respectively. The blue curve was obtained when the M-TX was held in a user's palm. Details about the positions of the M-TX are shown in Fig. 8. The dashed curves are the fitting curves obtained using (2), where the parameters used for calculating the fitting curves are summarized in Table I. Because the calculated data are fairly well fit to the measured data, it is considered that the circuit model shown in Fig. 3 is quite effective.

We also plotted three examples of the measured $G_e(f)$ in Fig. 6. The conditions adopted for measuring $G_e(f)$ are shown in Fig. 10. The black curve was obtained when the M-TX was held in the outsider's palm and $D = 0$ m. The green

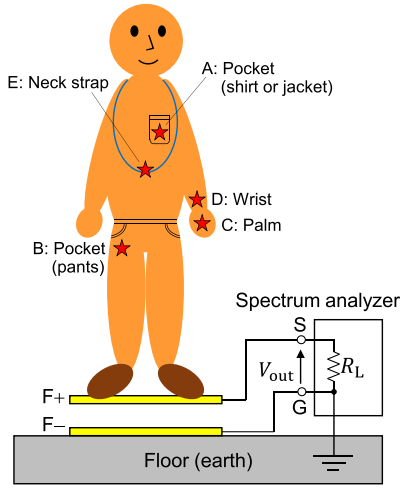

(a)

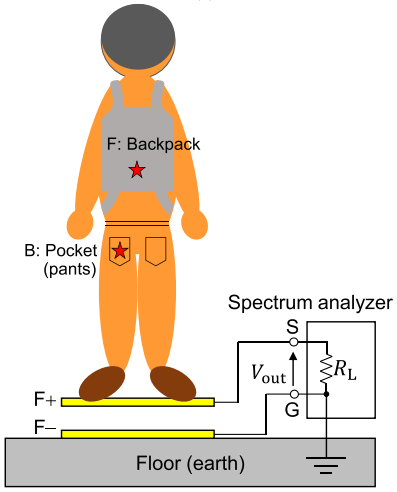

(b)

Fig. 8. Positions of an M-TX, which is a pair of electrodes M+ and M−, adopted for obtaining channel gain data under an ordinary state. The M-TX was attached to a person standing on the fixed electrode F+. The positions of the M-TX are indicated by stars. (a) Front view. (b) Back view.

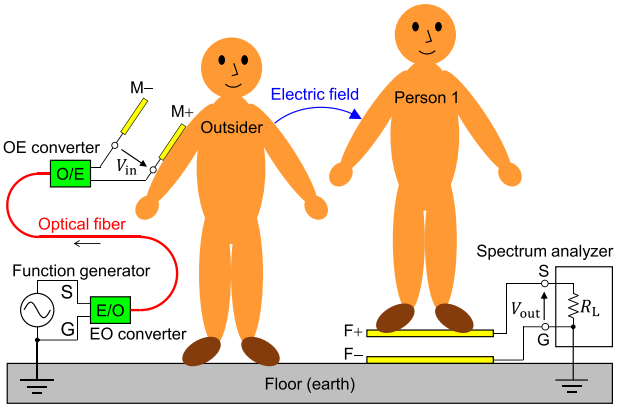

Fig. 9. Setup for evaluating HBC uplink channel gain by using EO/OE converters in an extraordinary state.

curve was obtained when the M-TX was attached to the outsider's wrist and $D = 0.5$ m. The blue curve was obtained when the M-TX was put in the outsider's pocket of pants

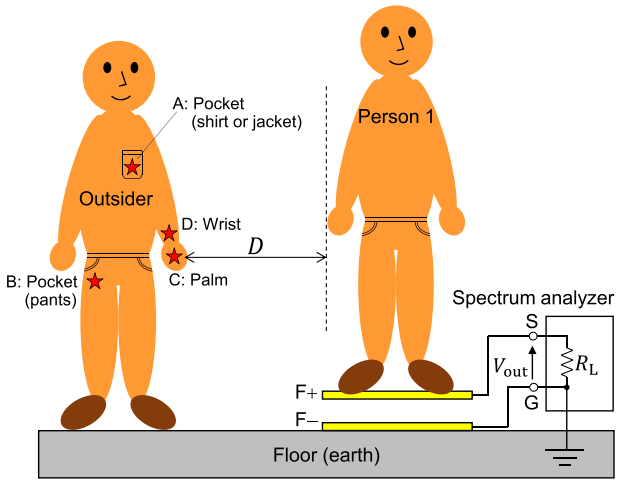

Fig. 10. Relationship between two persons adopted for obtaining channel gain data in an extraordinary state. The distance between M-TX and Person 1 is denoted by D. Measurements were done for $D = 0$, 0.2, 0.5, and 1.0 m.

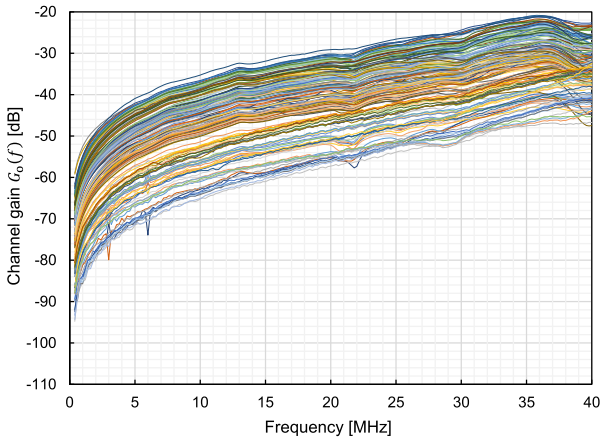

Fig. 11. All channel gain data measured in an ordinary state ($N = 180$).

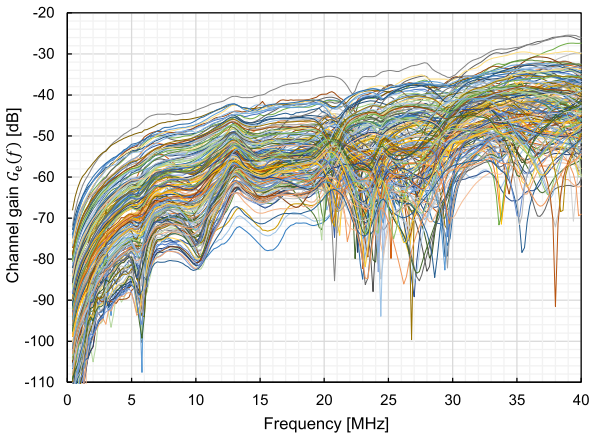

Fig. 12. All channel gain data measured in an extraordinary state ($N = 180$).

and $D = 0.5$ m. As shown by the blue and green curves, $G_e(f)$ tends to vary abruptly. On the other hand, as shown by the black curve, $G_e(f)$ sometimes becomes smooth and resembles $G_o(f)$. As indicated in Fig. 6, $G_e(f)$ exhibits

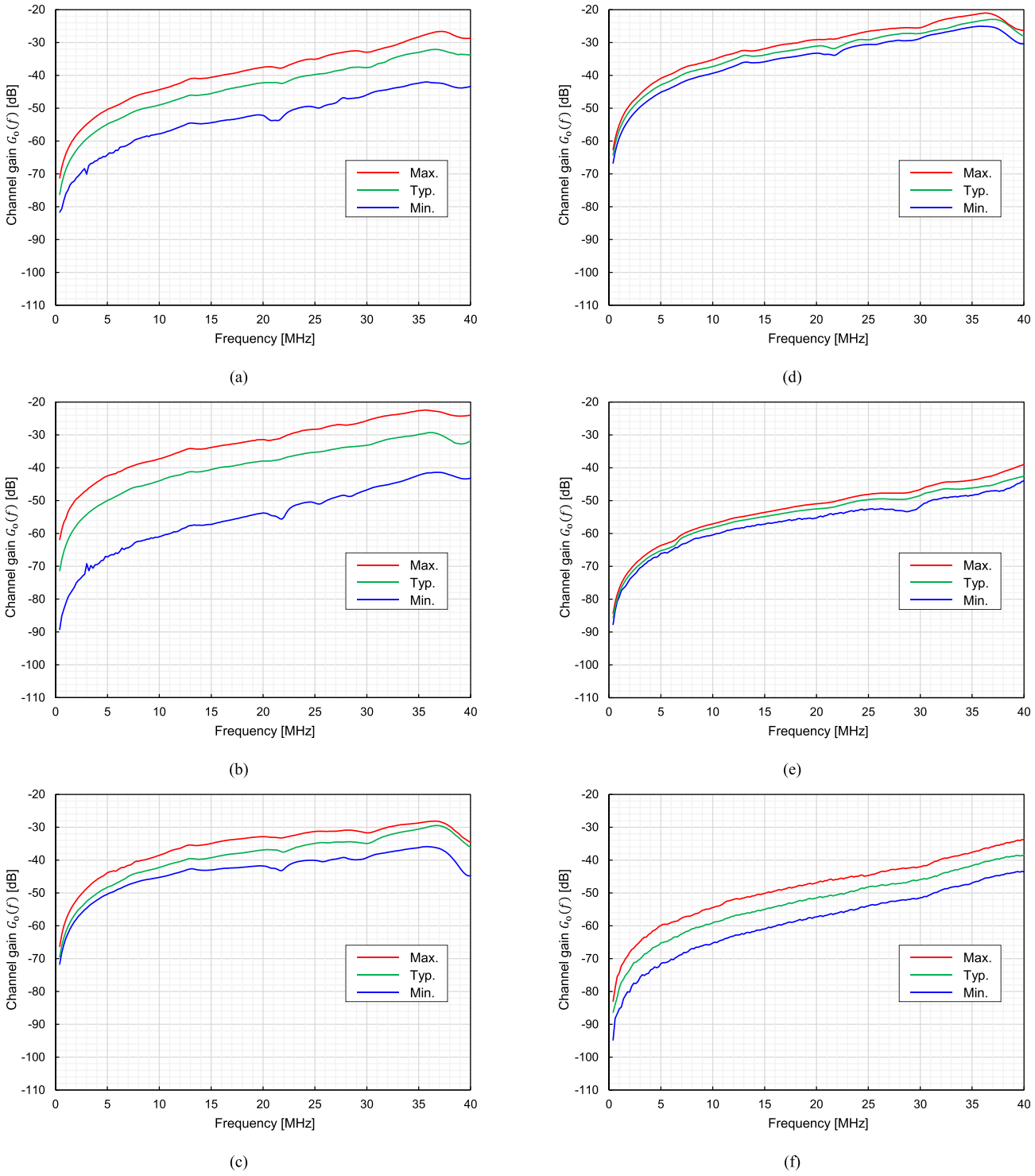

Fig. 13. Variation of channel gain features in an ordinary state measured when the M-TX was positioned at (a) condition A: pocket (shirt or jacket), (b) condition B: pocket (pants), (c) condition C: palm, (d) condition D: wrist, (e) condition E: neck strap, and (f) condition F: backpack. These positions are illustrated in Fig. 8. The maximum, typical, and minimum cases of $G_o(f)$ are excerpted from measured results and they are shown by red, green, and blue curves, respectively.

complex behavior. Furthermore, the abrupt variation of $G_e(f)$ could not be fit well by the calculated curves. This suggests that HBC systems under an extraordinary state possess some factors that cannot be expressed by the circuit model shown in Fig. 4. Although it is currently difficult to account for the origin of the abrupt variation, the remarkable feature of $G_e(f)$ is, however, advantageous for our purpose, that is, for classifying the measured $G(f)$ into $G_o(f)$ or $G_e(f)$.

III. Evaluation of Channel Gain Characteristics

In this section, we describe the evaluation of $G(f)$. As mentioned in Section II, an important feature of HBC systems

is that fixed devices are earthed, whereas mobile devices are electrically isolated from the earth. To correctly evaluate the channel gain characteristics, these conditions must be maintained during evaluation [10], [37], [38].

The experimental setup used for evaluating $G_{\mathrm{o}}(f)$ is shown in Fig. 7. A key point here is the use of optical devices, such as electrical-to-optical (EO)/optical-to-electrical (OE) converters. EO/OE converters make it possible to utilize useful commercial apparatus such as function generators. The electrical signals generated by the function generator are applied to the EO converter and converted into optical signals. The optical signals are then delivered to the OE converter by an optical fiber cable and reconverted into electrical signals, which are applied between M+ and M−. If the function generator is directly connected to the mobile electrodes, M− will inevitably be earthed. In this situation, it is impossible to correctly evaluate the HBC channel characteristics. Because of the isolated nature of the optical fiber cable, it is possible to imitate a battery-driven M-TX with a function generator driven by an ac power cord. Furthermore, we used a spectrum analyzer instead of F-RX. Hence, it is possible to obtain $G_{\mathrm{o}}(f)$ by sweeping the signal frequencies of the function generator. To obtain $G_{\mathrm{o}}(f)$ under various conditions, we measured it by changing the positions of the pair of mobile electrodes, M+ and M−, which were attached to a person standing on F+. The positions of the electrode pair are indicated by the stars in Fig. 8. The measurement of $G_{\mathrm{o}}(f)$ was done with four different subjects wearing their own clothes and shoes.

We also evaluated $G_{\mathrm{e}}(f)$ using the setup shown in Fig. 9. In this setup, M+ and M− are attached to the outsider. In addition to the evaluation of $G_{\mathrm{o}}(f)$, we evaluated $G_{\mathrm{e}}(f)$ at various positions of the electrode pair attached to the outsider. Furthermore, we measured $G_{\mathrm{e}}(f)$ for various distances ($D =$ 0, 0.2, 0.5, and 1.0 m), where D is the distance between the M-TX and Person 1, as shown in Fig. 10. The measurement of $G_{\mathrm{e}}(f)$ was done with five different subjects wearing their own clothes and shoes.

All $G_{\mathrm{o}}(f)$ and $G_{\mathrm{e}}(f)$ curves obtained in our experiments are shown in Figs. 11 and 12, respectively. In both cases, the number of data samples N was 180. The data were obtained in the frequency range from 0.4 to 40 MHz with a frequency resolution of 0.2 MHz. Therefore, each curve of $G(f)$ is composed of 199 points. It is observed that $G_{\mathrm{o}}(f)$ tends to be smooth and $G_{\mathrm{e}}(f)$ tends to vary abruptly. Therefore, at first glance, it seems easy to correctly classify unknown $G(f)$ into $G_{\mathrm{o}}(f)$ or $G_{\mathrm{e}}(f)$.

Fig. 13 shows variation of $G_{\mathrm{o}}(f)$ measured for different positions of the M-TX. It is observed that the channel gain variations depend on positions of the M-TX. As shown in Fig. 13(d) and (e), the variation becomes smaller when the M-TX is attached to a wrist and held with a neck strap. This is because, for these cases, the coupling between M+ and body is maintained large and that between M− and body is maintained small. On the other hand, as indicated in Fig. 13(b), the variation becomes large, especially when the M-TX is put in a pant pocket. This variation is caused by the fact that it depends on the size and position of the pockets on the user's pants. In this case, the coupling between M+ and body depends on the pants. Furthermore, the degree of coupling between M− and body, which is usually user's arm, strongly depends on the situations. Although the average values of $G_{\mathrm{o}}(f)$ largely depend on positions of the M-TX, it is again confirmed that $G_{\mathrm{o}}(f)$ always possesses smooth features. It is considered that the smooth features of $G_{\mathrm{o}}(f)$ are advantageous for our purpose, e.g., classification of $G(f)$.

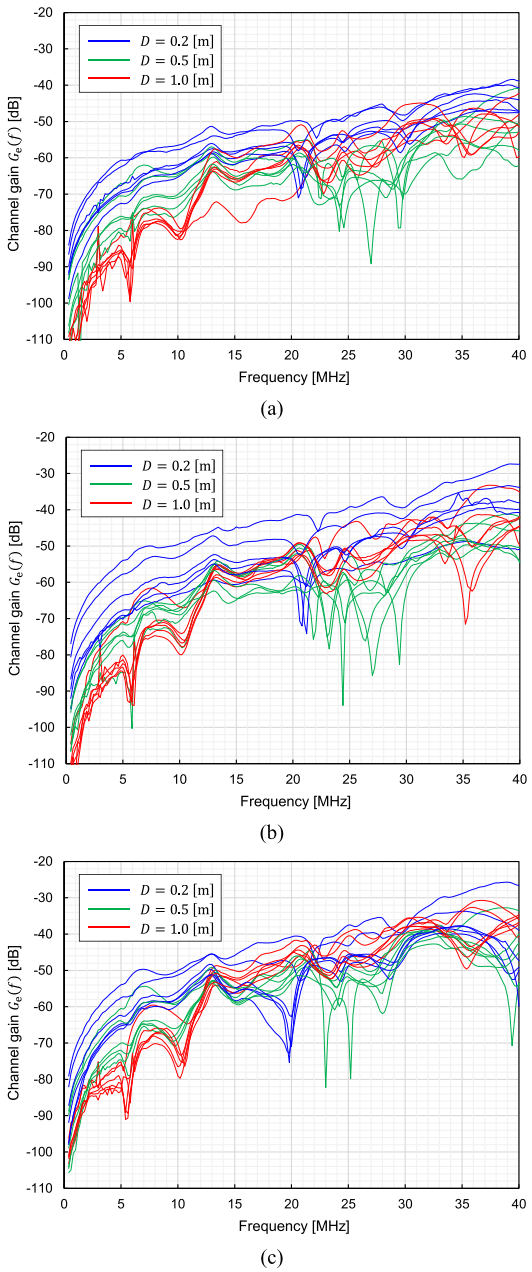

Fig. 14. Examples of channel gain features in an extraordinary state measured when the M-TX was positioned at (a) condition A: pocket (shirt or jacket), (b) condition B: pocket (pants), and (c) condition D: wrist. These positions are illustrated in Fig. 10. The blue, green, and red curves were obtained when $D = 0.2$, 0.5, and 1.0 m, respectively.

Fig. 14 shows examples of $G_{\mathrm{e}}(f)$ measured when the M-TX was attached to three different positions, which are shirt or jacket pockets, pant pockets, and wrist. These positions are illustrated in Fig. 10. The blue, green, and red curves correspond to $G_{\mathrm{e}}(f)$ measured when D equals 0.2, 0.5, and 1.0 m,

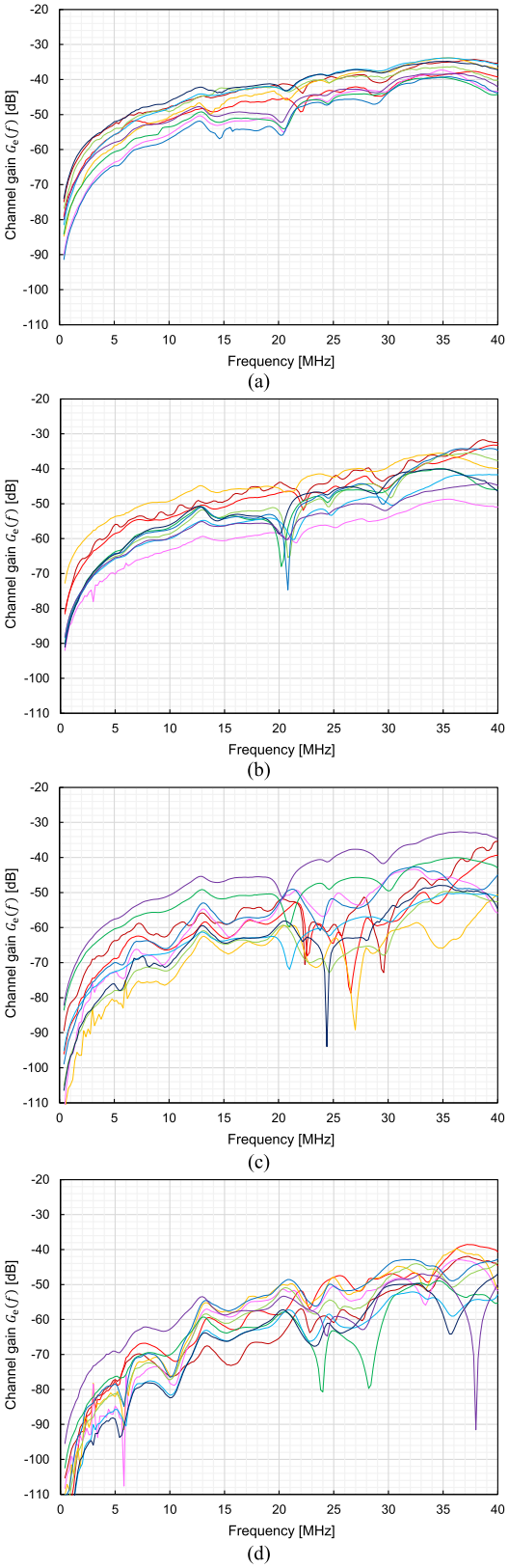

Fig. 15. Examples of channel gain features in an extraordinary state measured when (a) $D = 0$ m, (b) $D = 0.2$ m, (c) $D = 0.5$ m, and (d) $D = 1.0$ m.

respectively. When $D = 0.2$ m, $G_e(f)$ usually shows smooth features. Remarkable features of $G_e(f)$ measured when $D = 0.5$ m are the dips existing between 20 and 30 MHz. When

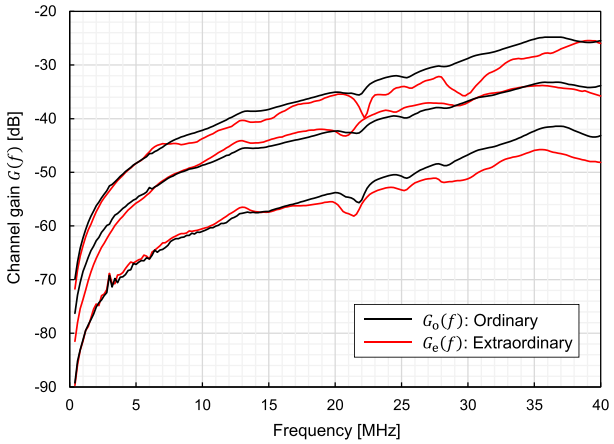

Fig. 16. Examples of channel gain features measured in ordinary and extraordinary states. As shown in this figure, the features of $G_e(f)$ (red curves) sometimes become quite similar to that of $G_o(f)$ (black curves). Therefore, it is not always easy to classify the measured $G(f)$ correctly into $G_o(f)$ or $G_e(f)$.

D is increased to 1.0 m, frequencies of the dips shift lower and gain below about 10 MHz tends to decrease. It is observed from Fig. 14 that the tendency of the channel gain variation depending on D is common to all positions of the M-TX.

To clearly see the relationship between D and features of $G_e(f)$, we plotted examples of measured $G_e(f)$ for each D in Fig. 15. When $D = 0$ m, $G_e(f)$ are smooth and resembling $G_o(f)$. As D increases, the variation of $G_e(f)$ becomes larger and peaky dips are often observed; however, the peaky dips do not always appear even for the larger D.

As seen in Figs. 14 and 15, $G_e(f)$ tends to show abrupt variation; however, it is also observed that even $G_e(f)$ sometimes possess smooth features and resembles $G_o(f)$ especially for smaller D values. To clearly show this fact, we plotted examples of measured $G_e(f)$ resembling $G_o(f)$ in Fig. 16. As shown in this figure, the features of $G_e(f)$ sometimes become quite similar to that of $G_o(f)$. In this case, it is not easy to classify the measured $G(f)$ correctly into $G_o(f)$ or $G_e(f)$. Therefore, the binary classification problem that must be solved is not trivial.

IV. Binary Classification of Channel Gain Data

Our purpose was to predict the existence of an outsider based on the measured $G(f)$. This is equivalent to classifying the measured $G(f)$ into $G_o(f)$ or $G_e(f)$, which is a binary classification problem. In this section, we explain the methods and classification results in detail.

As it is well known that machine learning is effective for solving classification problems, we adopted a machine learning approach to our purpose [37], [38], [39], [40], [41], [42]. Although there are various machine learning methods, k-NN is widely known as a simple method [39]. In this study, we adopted k-NN as the machine learning method. Although k-NN is a simple method, excellent performance can be obtained by appropriately preprocessing the channel gain data.

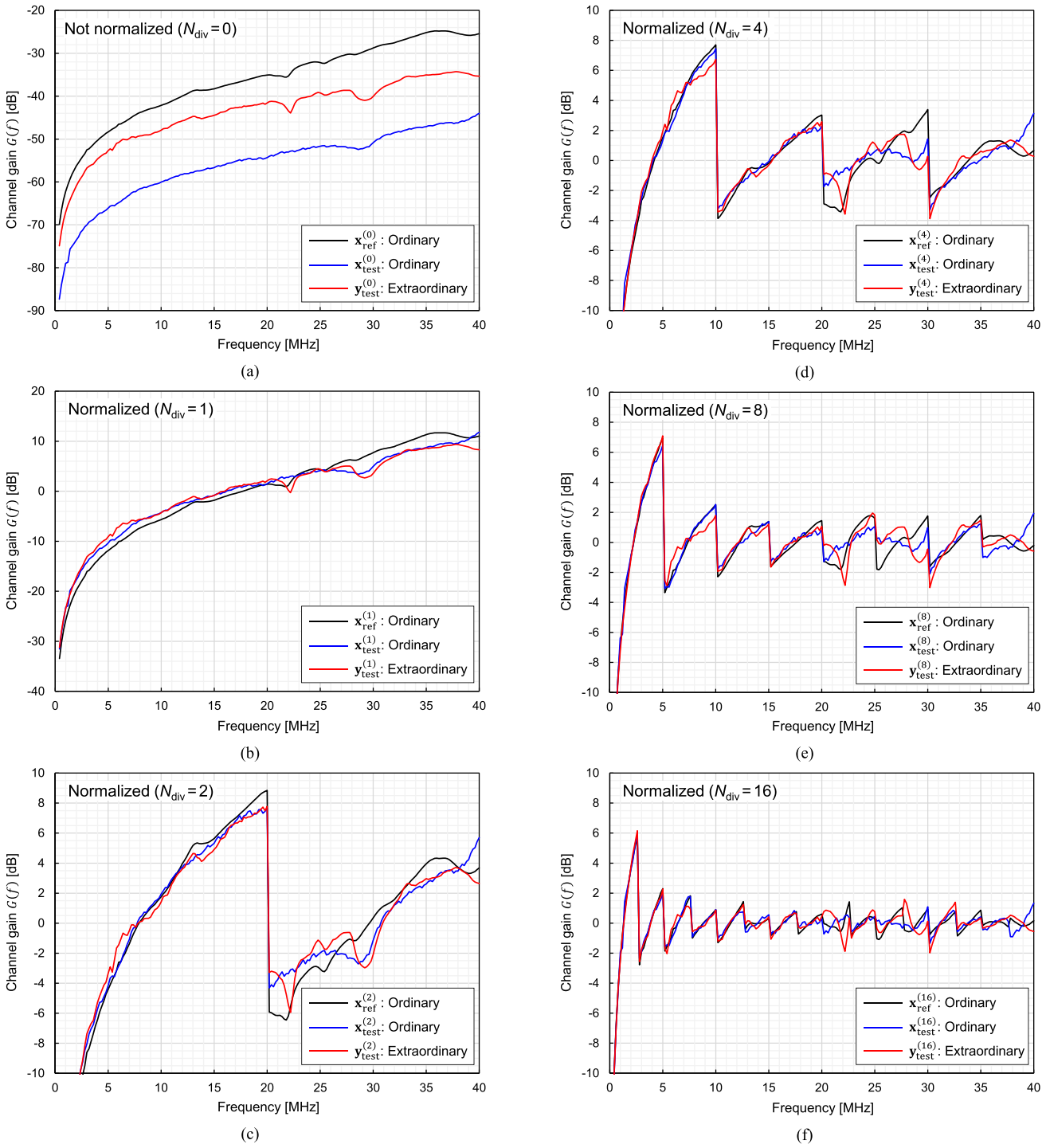

Fig. 17. Three examples of channel gain data ($\mathbf{x}_{ref}$, $\mathbf{x}_{test}$, $\mathbf{y}_{test}$) preprocessed by our proposed method. (a) Not normalized. (b) Normalized ($N_{div} = 1$). (c) Normalized ($N_{div} = 2$). (d) Normalized ($N_{div} = 4$). (e) Normalized ($N_{div} = 8$). (f) Normalized ($N_{div} = 16$). Without preprocessing, an undesirable situation, $d_p(\mathbf{x}_{test}, \mathbf{x}_{ref}) > d_p(\mathbf{y}_{test}, \mathbf{x}_{ref})$, often occurred similar to (a). After preprocessing, the undesirable situation is improved, i.e., $d_p(\mathbf{x}_{test}, \mathbf{x}_{ref}) \approx d_p(\mathbf{y}_{test}, \mathbf{x}_{ref})$. Finally, for larger N_{div}, a desirable situation, $d_p(\mathbf{x}_{test}, \mathbf{x}_{ref}) < d_p(\mathbf{y}_{test}, \mathbf{x}_{ref})$, appears to be realized.

A. *k-NN Classification*

In this subsection, we explain the application of k-NN to our classification problem.

Because all measured data of $G_o(f)$ and $G_e(f)$ consist of 199 components, we denote nth data of the measured $G_o(f)$ and $G_e(f)$ by 199-D vectors $\mathbf{x}_n$ and $\mathbf{y}_n$, respectively. In the component representation, the data vectors $\mathbf{x}_n$ and $\mathbf{y}_n$ are expressed as

$$\mathbb{X} \ni \mathbf{x}_n = (x_{n1}, x_{n2}, x_{n3}, \ldots, x_{n199}) \tag{4}$$

$$\mathbb{Y} \ni \mathbf{y}_n = (y_{n1}, y_{n2}, y_{n3}, \ldots, y_{n199}) \tag{5}$$

where $\mathbb{X}$ and $\mathbb{Y}$ are data sets composed of $G_o(f)$ and $G_e(f)$ measured beforehand, respectively. Both $\mathbb{X}$ and $\mathbb{Y}$ can be considered training datasets. As explained in Section III,

we experimentally obtained 180 data samples for both $\mathbf{x}_n$ and $\mathbf{y}_n$. Therefore, the training datasets can be written as

$$\mathbb{X} = \{\mathbf{x}_1, \mathbf{x}_2, \ldots, \mathbf{x}_{180}\} \tag{6}$$

$$\mathbb{Y} = \{\mathbf{y}_1, \mathbf{y}_2, \ldots, \mathbf{y}_{180}\}. \tag{7}$$

Furthermore, we define the appropriate distance between two arbitrary vectors $\mathbf{u}$ and $\mathbf{v}$. In this study, we adopt the p-norm to define the distance as

$$d_p(\mathbf{u}, \mathbf{v}) \triangleq \|\mathbf{u} - \mathbf{v}\|_p = \left(\sum_{i=1}^{199} |u_i - v_i|^p \right)^{1/p} \tag{8}$$

where u_i and v_i are components of $\mathbf{u}$ and $\mathbf{v}$, respectively.

The k-NN classifier used in our study is considered to be a function that outputs 0 or 1 when a new unknown data vector $\mathbf{z}$ is input. Mathematically, the k-NN classifier can be written as follows:

$$C_p^k(\mathbf{z}; \mathbb{X} \cup \mathbb{Y}) = \begin{cases} 0, & \text{if } N_\mathrm{x} > N_\mathrm{y} \\ 1, & \text{else} \end{cases} \tag{9}$$

where N_x and N_y are calculated by the procedure listed below.

Procedure 1:

1) Let $\mathbb{D}$ be a set composed of $d_p(\mathbf{z}, \mathbf{v})$ calculated for all $\mathbf{v} \in \mathbb{X} \cup \mathbb{Y}$. $d_p(\mathbf{z}, \mathbf{v})$ is regarded as an error function.
2) Find the k-smallest values of $d_p(\mathbf{z}, \mathbf{v}) \in \mathbb{D}$ and create a set $\{d_p^{(1)}, d_p^{(2)}, \ldots, d_p^{(k)}\}$ composed of the values.
3) Create a set $\{\mathbf{v}^{(1)}, \mathbf{v}^{(2)}, \ldots, \mathbf{v}^{(k)}\}$ composed of the k vectors, where $\mathbf{v}^{(i)}$ satisfies $d_p^{(i)} = d_p(\mathbf{z}, \mathbf{v}^{(i)})$ for $i = 1, 2, \ldots, k$.
4) Count N_x and N_y, which are the numbers of elements $\mathbf{v}^{(i)}$ contained in $\mathbb{X}$ and $\mathbb{Y}$, respectively.

B. Preprocessing of Channel Gain Data

As explained above, the k-NN classifier searches vectors that resemble the input vector from the training data sets $\mathbb{X}$ and $\mathbb{Y}$. The degree of resemblance is quantitatively evaluated using d_p. To obtain correct results with k-NN, it is desirable that the input vectors obtained under an ordinary state resemble vectors contained in $\mathbb{X}$. Similarly, the input vectors obtained under an extraordinary state should resemble vectors in $\mathbb{Y}$. These desirable situations are, however, not always realized.

Fig. 17(a) shows three examples of $G(f)$ obtained in our experiment. The black curve shows a typical feature of $G_\mathrm{o}(f)$ and we name it $\mathbf{x}_\mathrm{ref}$. Let us suppose two different test data $\mathbf{x}_\mathrm{test}$ and $\mathbf{y}_\mathrm{test}$, which were obtained under ordinary and extraordinary states and are plotted by blue and red curves, respectively. In this case, it is obvious that an undesirable situation $d_p(\mathbf{x}_\mathrm{test}, \mathbf{x}_\mathrm{ref}) > d_p(\mathbf{y}_\mathrm{test}, \mathbf{x}_\mathrm{ref})$ occurs. The k-NN classifier outputs incorrect results in these situations.

The preprocessing of channel gain data is required to prevent the occurrence of the undesirable situations. A simple preprocessing method is normalization, that is, offsetting a data vector with the average value of its components. In equation form, the normalization of a data vector $\mathbf{v}$ is expressed by the transformation

$$\begin{aligned} \mathbf{v} &= (v_1, v_2, \ldots, v_{199}) \\ \longmapsto \mathbf{v}^{(1)} &= (v_1 - v_\mathrm{av}, v_2 - v_\mathrm{av}, \ldots, v_{199} - v_\mathrm{av}) \end{aligned} \tag{10}$$

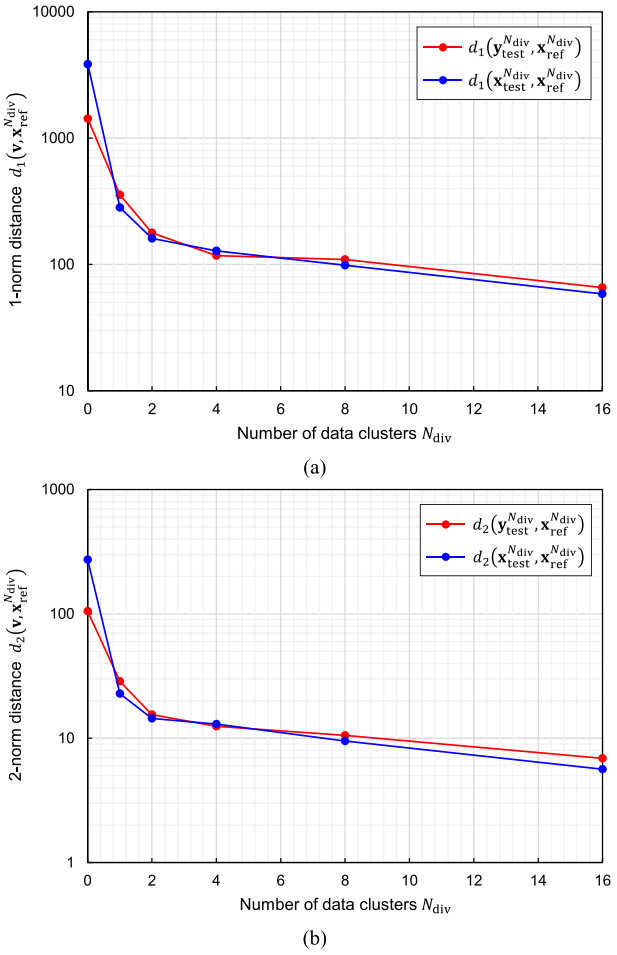

Fig. 18. (a) 1-norm distance d_1 and (b) 2-norm distance d_2 calculated for the channel gain data shown in Fig. 17. It is confirmed that the desirable situation, i.e., $d_p(\mathbf{x}_\mathrm{test}, \mathbf{x}_\mathrm{ref}) < d_p(\mathbf{y}_\mathrm{test}, \mathbf{x}_\mathrm{ref})$, is realized by the normalization and partition ($N_\mathrm{div} \geq 8$) of channel gain data.

$$v_\mathrm{av} \triangleq \frac{1}{199} \sum_{i=1}^{199} v_i \tag{11}$$

where $\mathbf{v}^{(1)}$ is the normalized data vector. The normalized data vectors $\mathbf{x}_\mathrm{ref}^{(1)}$, $\mathbf{x}_\mathrm{test}^{(1)}$, and $\mathbf{y}_\mathrm{test}^{(1)}$, which, respectively, correspond to $\mathbf{x}_\mathrm{ref}$, $\mathbf{x}_\mathrm{test}$, and $\mathbf{x}_\mathrm{test}$, are plotted in Fig. 17(b). It is observed that the situation become more preferable than that in Fig. 17(a) because $d_p(\mathbf{x}_\mathrm{test}^{(1)}, \mathbf{x}_\mathrm{ref}^{(1)}) \approx d_p(\mathbf{y}_\mathrm{test}^{(1)}, \mathbf{x}_\mathrm{ref}^{(1)})$ in Fig. 17(b).

However, as seen later, even the situation shown in Fig. 17(b) is insufficient for obtaining high-performance classifiers. The following data preprocessing procedure is used to realize the desirable situation $d_p(\mathbf{x}_\mathrm{test}, \mathbf{x}_\mathrm{ref}) < d_p(\mathbf{y}_\mathrm{test}, \mathbf{x}_\mathrm{ref})$.

Procedure 2:

1) Choose a natural number N_div.
2) Partition the components of a data vector $\mathbf{v}$ into N_div clusters.
3) Normalize each cluster.
4) Remove the partition.

Let $\mathbf{v}^{(N_\mathrm{div})}$ denote the data vectors transformed from $\mathbf{v}$ using the procedure mentioned above. Note that data vectors such as $\mathbf{x}_\mathrm{ref}^{(1)}$, $\mathbf{x}_\mathrm{test}^{(1)}$, and $\mathbf{y}_\mathrm{test}^{(1)}$ are special cases of $N_\mathrm{div} = 1$, which

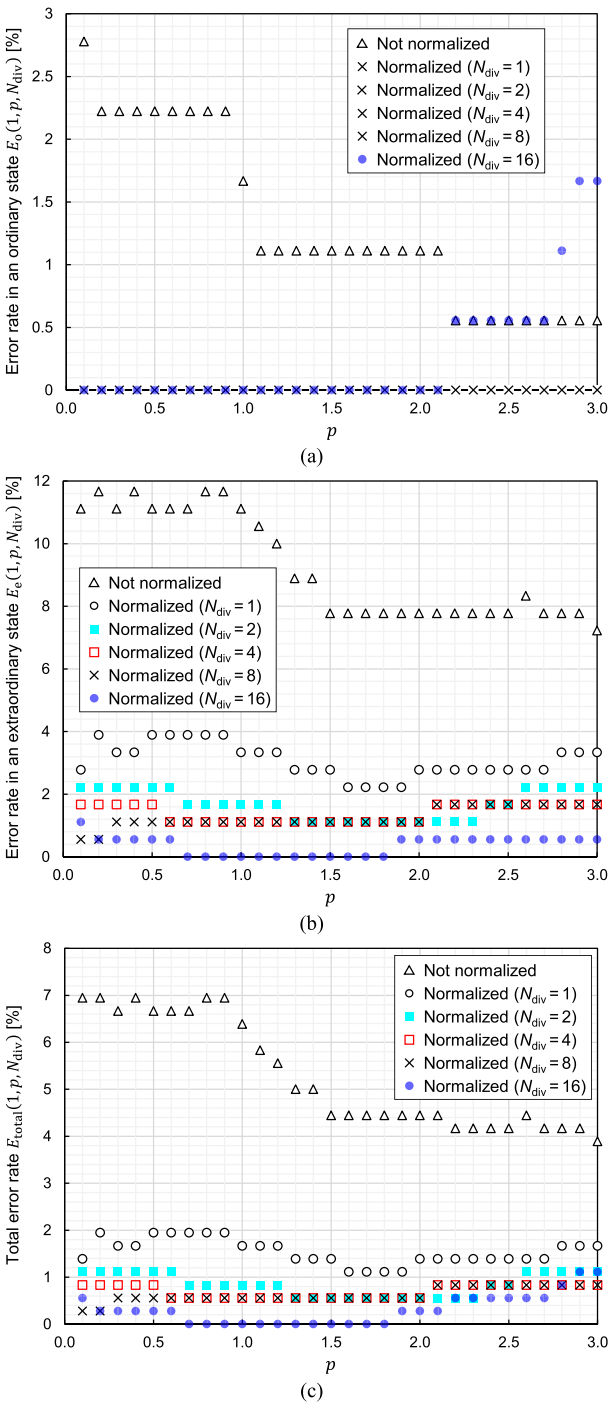

Fig. 19. Error rates obtained with 1-NN classifiers. (a) Error rates E_o evaluated in an ordinary state. (b) Error rates E_e evaluated in an extraordinary state. (c) Total error rates E_{total}.

indicates no partition. Furthermore, we define $\mathbf{v}^{(0)} \triangleq \mathbf{v}$, which implies that the data vector is not normalized.

The data vectors preprocessed using *Procedure 2* are plotted in Fig. 17 for several values of N_{div}. It appears that the desirable situation $d_p(\mathbf{x}_{test}^{(N_{div})}, \mathbf{x}_{ref}^{(N_{div})}) < d_p(\mathbf{y}_{test}^{(N_{div})}, \mathbf{x}_{ref}^{(N_{div})})$ is obtained for $N_{div} = 16$ at a glance. To confirm the validity of preprocessing, we plotted d_1 and d_2 for various N_{div} values in Fig. 18(a) and (b), respectively. It was confirmed that the

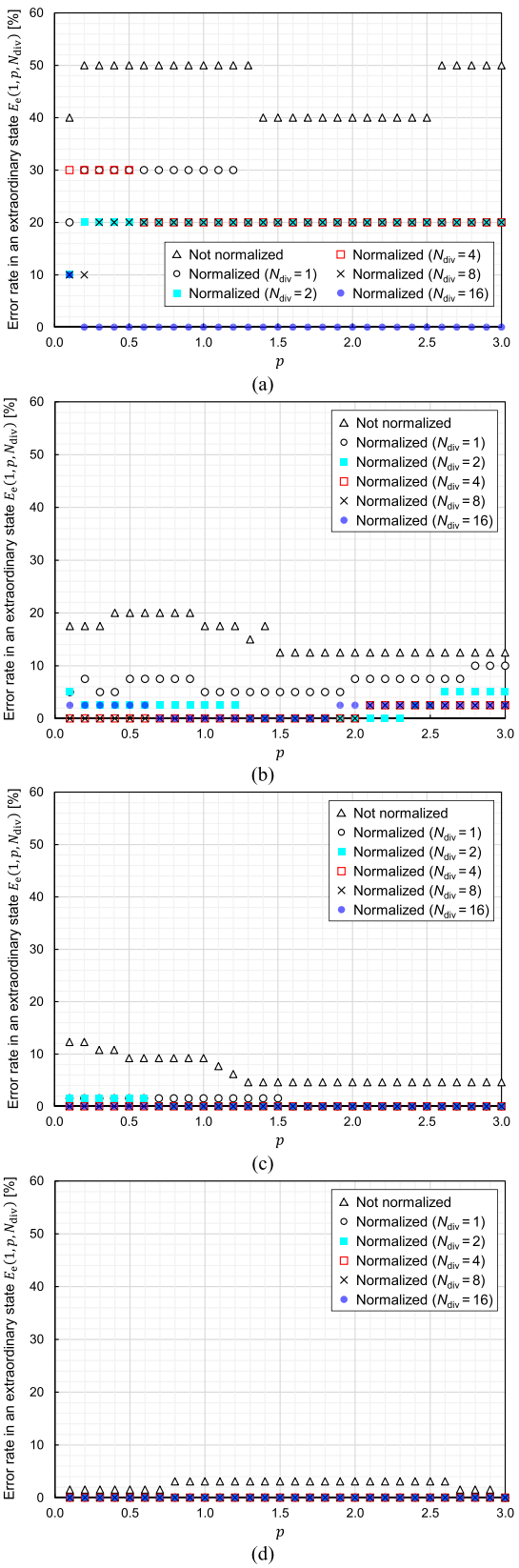

Fig. 20. Error rates E_e obtained with 1-NN classifiers in an extraordinary state when (a) $D = 0$ m, (b) $D = 0.2$ m, (c) $D = 0.5$ m, and (d) $D = 1.0$ m.

desirable situation $d_p(\mathbf{x}_{test}^{(N_{div})}, \mathbf{x}_{ref}^{(N_{div})}) < d_p(\mathbf{y}_{test}^{(N_{div})}, \mathbf{x}_{ref}^{(N_{div})})$ is realized for $p = 1, 2$ when $N_{div} \geq 8$ in the sample data shown in Fig. 17.

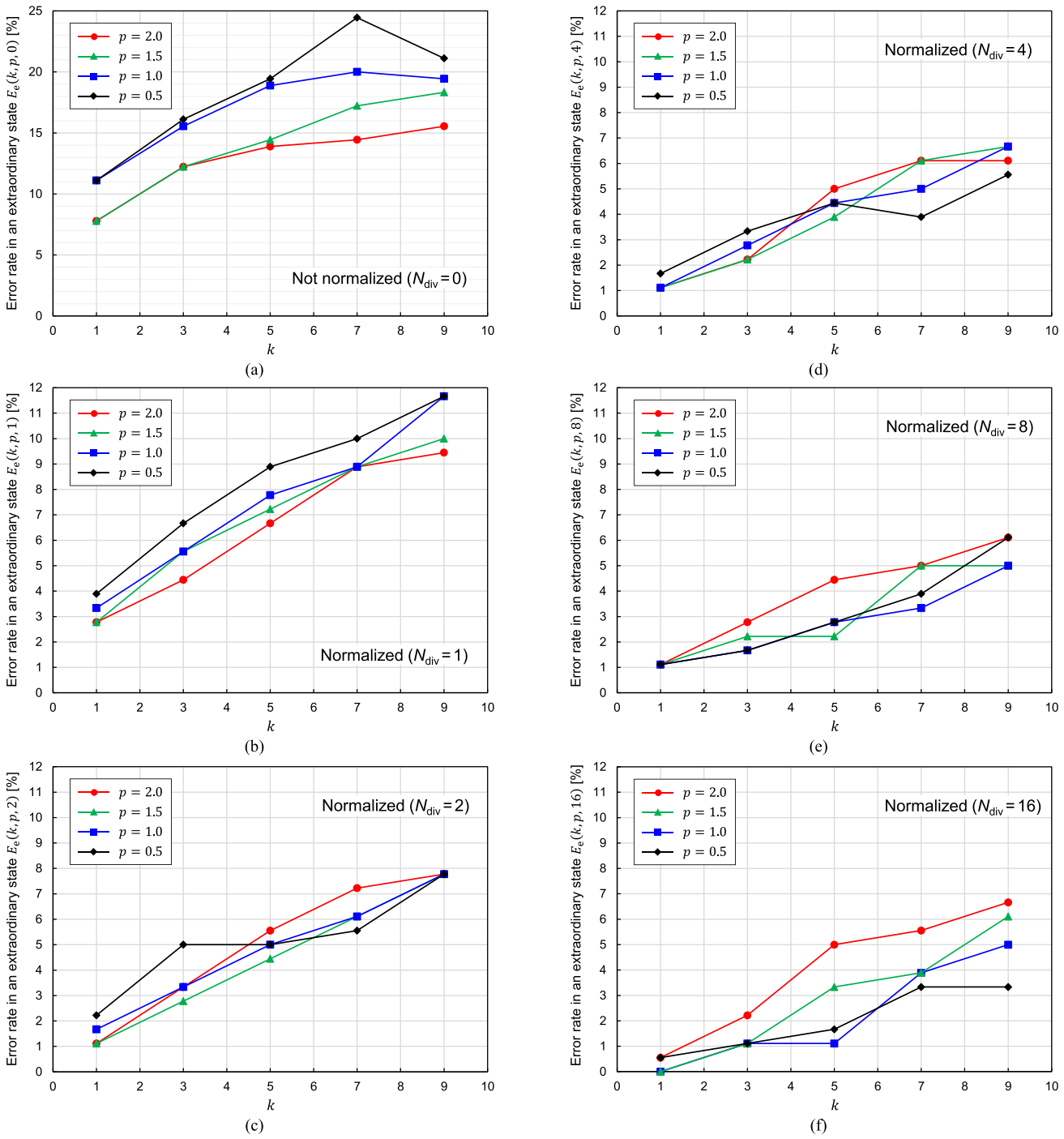

Fig. 21. Relationship between the error rate E_e obtained in an extraordinary state and the values of k (in k-NN classifiers). These figures were obtained when (a) $N_{div} = 0$, (b) $N_{div} = 1$, (c) $N_{div} = 2$, (d) $N_{div} = 4$, (a) $N_{div} = 8$, and (f) $N_{div} = 16$. It is observed that E_e becomes minimum when $k = 1$ regardless of the parameters p and N_{div}. This means that 1-NN is the best of all k-NN classifiers.

C. Performance Evaluation of k-NN Classifiers

This subsection describes the methods and results of evaluating the performance of k-NN classifiers.

To evaluate the performance of k-NN classifiers, we utilized leave-one-out cross-validation (LOOCV) [39]. As explained previously, we experimentally obtained channel gain datasets $\mathbb{X}$ and $\mathbb{Y}$ both comprising 180 samples. For simplicity, we use the symbols $\mathbb{X}$ and $\mathbb{Y}$ not only for sets composed of $\mathbf{x}_i$ and $\mathbf{y}_i$ but also for those composed of $\mathbf{x}_i^{(N_{div})}$ and $\mathbf{y}_i^{(N_{div})}$. To execute LOOCV, we should pick up one data vector $\mathbf{x}_i^{(N_{div})}$ (or $\mathbf{y}_i^{(N_{div})}$) as a test sample from the datasets. Then, the datasets from which the picked-up data vector is excluded are used as the training datasets. In equation form, the outputs of the k-NN classifier for the input test vectors $\mathbf{x}_i^{(N_{div})}$ and $\mathbf{y}_i^{(N_{div})}$ are, respectively, written as

$$C_p^k\left(\mathbf{x}_i^{(N_{div})}; (\mathbb{X} \cup \mathbb{Y}) - \left\{\mathbf{x}_i^{(N_{div})}\right\}\right) \tag{12}$$

$$C_p^k\left(\mathbf{y}_i^{(N_{div})}; (\mathbb{X} \cup \mathbb{Y}) - \left\{\mathbf{y}_i^{(N_{div})}\right\}\right). \tag{13}$$

Then, the error rates obtained with LOOCV for the input data of the ordinary and extraordinary states can be, respectively, written as

$$E_{\mathrm{o}}(k, p, N_{\mathrm{div}}) = \frac{1}{180}\sum_{i=1}^{180} C_p^k\left(\mathbf{x}_i^{(N_{\mathrm{div}})}; (\mathbb{X}\cup\mathbb{Y}) - \left\{\mathbf{x}_i^{(N_{\mathrm{div}})}\right\}\right) \quad (14)$$

$$E_{\mathrm{e}}(k, p, N_{\mathrm{div}}) = \frac{1}{180}\sum_{i=1}^{180}\left[1 - C_p^k\left(\mathbf{y}_i^{(N_{\mathrm{div}})}; (\mathbb{X}\cup\mathbb{Y}) - \left\{\mathbf{y}_i^{(N_{\mathrm{div}})}\right\}\right)\right]. \quad (15)$$

Furthermore, the total error rate regarding all the 360 data samples is written as

$$E_{\mathrm{total}}(k, p, N_{\mathrm{div}}) = \frac{1}{2}\{E_{\mathrm{o}}(k, p, N_{\mathrm{div}}) + E_{\mathrm{e}}(k, p, N_{\mathrm{div}})\}. \quad (16)$$

As shown later, 1-NN is found to be the best of all k-NN classifiers. Hence, we plotted the error rates for 1-NN classifiers, as shown in Fig. 19. As shown in Fig. 19(a), $E_{\mathrm{o}}(1, p, N_{\mathrm{div}})$ reaches zero for most combinations of $\{p, N_{\mathrm{div}}\}$ by simply applying normalization. As a result, it can be said that the classification in an ordinary state is easy. However, Fig. 19(b) shows that the detection of an extraordinary state is not easy because $E_{\mathrm{e}}(1, p, N_{\mathrm{div}})$ reaches zero only for limited combinations of $\{p, N_{\mathrm{div}}\}$. In equation form, the condition under which E_{e} reaches zero can be written as

$$\begin{cases} 0.7 \le p \le 1.8 \\ N_{\mathrm{div}} = 16. \end{cases} \quad (17)$$

Although the classification of $G_{\mathrm{e}}(f)$ is more difficult than that of $G_{\mathrm{o}}(f)$, error-free classification was achieved with the above conditions. An important result obtained here is that the 1-norm (Manhattan distance) is more suitable than the 2-norm (Euclidean distance) for calculating the error function d_p in the proposed method. Fig. 19(c) shows the total error rate E_{total}. It is observed that $E_{\mathrm{total}}(1, p, N_{\mathrm{div}}) = E_{\mathrm{e}}(1, p, N_{\mathrm{div}})/2$ for the most combinations of $\{p, N_{\mathrm{div}}\}$ because $E_{\mathrm{o}}(1, p, N_{\mathrm{div}}) = 0$ for the combinations.

Although it was demonstrated that the classification of $G_{\mathrm{e}}(f)$ is more difficult than that of $G_{\mathrm{o}}(f)$, Fig. 15 implies that the difficulty of the classification depends on D. It is expected that the classification of $G_{\mathrm{e}}(f)$ will be easy for $D \ge 0.5$ m because most $G_{\mathrm{e}}(f)$ in Fig. 15(c) and (d) do not resemble $G_{\mathrm{o}}(f)$ in shape. On the other hand, the classification will be much more difficult for $D \le 0.2$ m because $G_{\mathrm{e}}(f)$ in Figs. 15(a) and (b) tend to resemble $G_{\mathrm{o}}(f)$ in shape. To clarify the concern, we plotted E_{e} for each D value in Fig. 20. As we expected, error-free classification was achieved for most combinations of $\{p, N_{\mathrm{div}}\}$ when $D \ge 0.5$ m and it was achieved for the limited combinations of $\{p, N_{\mathrm{div}}\}$ when $D \le 0.2$ m.

Finally, we investigated the influence of k on E_{e}. For this, we plotted E_{e} as a function of k in Fig. 21. It is observed that E_{e} is an almost monotonously increasing function of k and becomes minimum when $k = 1$ for all combinations of $\{p, N_{\mathrm{div}}\}$. Therefore, it can be concluded that 1-NN is the best k-NN classifier.

V. Conclusion

We proposed and investigated methods for predicting the existence of an outsider in HBC systems based on channel gain features detected by a F-RX. This approach is effective in resolving the problem of HBC system security, which leads to accidental data transmission and misidentification. We experimentally obtained 360 samples of HBC-channel gain data with EO/OE converters, which are effective for correctly evaluating HBC channel characteristics. It is a binary classification problem that predicts the existence of an outsider based on channel gain information. The experimental data implies that the classification problem becomes more difficult as D, which is the distance between the outsider and rightful user, decreases. We adopted k-NN to solve the classification problem and proposed an effective method to preprocess the training data. It was revealed that 1-norm performs better than 2-norm in calculating error functions, and 1-NN is the best of all k-NN classifiers. It was demonstrated that the error rate of the binary classification reached zero even for $D = 0$ m with the method and parameters that we found.

In this study, we utilized a broad bandwidth of 0.4–40 MHz. However, it is preferable for the bandwidth required for classification to become narrower. Therefore, the next meaningful step is to determine the optimal frequency bands and minimum bandwidth required for high-performance classification. Machine learning technologies have become astonishingly powerful and are increasingly evolving. It might be valuable to examine the effectiveness of various machine learning methods, such as artificial neural networks, in HBC systems.

References

[1] T. G. Zimmerman, "Personal area networks: Near-field intrabody communication," *IBM Syst. J.*, vol. 35, no. 3, pp. 609–617, 1996.

[2] M. Fukumoto and Y. Tonomura, "'Body coupled FingerRing': Wireless wearable keyboard," in *Proc. ACM SIGCHI Conf. Human Factors Comput. Syst.*, Atlanta, GA, USA, Mar. 1997, pp. 147–154.

[3] N. Matsushita, S. Tajima, Y. Ayatsuka, and J. Rekimoto, "Wearable key: Device for personalizing nearby environment," in *Dig. Papers. 4th Int. Symp. Wearable Comput.*, Atlanta, GA, USA, 2000, pp. 119–126.

[4] K. Partridge et al., "Empirical measurements of intrabody communication performance under varied physical configurations," in *Proc. 14th Annu. ACM Symp. User Interface Softw. Technol. (UIST)*, Orlando, FL, USA, 2001, pp. 183–190.

[5] M. Shinagawa, M. Fukumoto, K. Ochiai, and H. Kyuragi, "A near-field-sensing transceiver for intrabody communication based on the electrooptic effect," *IEEE Trans. Instrum. Meas.*, vol. 53, no. 6, pp. 1533–1538, Dec. 2004.

[6] Y. Kado and M. Shinagawa, "RedTacton near-body electric-field communications technology and its applications," *NTT Tech. Rev.*, vol. 8, no. 3, pp. 1–6, Mar. 2010.

[7] R. Kawano, F. Morisawa, M. Shinagawa, and Y. Kado, "LSIs for an advanced compact electric-field communication module," *NTT Tech. Rev.*, vol. 8, no. 3, pp. 1–6, Mar. 2010.

[8] A. Sasaki, R. Kawano, T. Ishihara, and M. Shinagawa, "Modeling of human-body near-field communication and evaluation of communication quality," *NTT Tech. Rev.*, vol. 8, no. 3, pp. 1–6, Mar. 2010.

[9] H. Goromaru, M. Ikeda, and Y. Hosoda, "Firmware technology for human-body communication," *NTT Tech. Rev.*, vol. 8, no. 3, pp. 1–6, Mar. 2010.

[10] A. Sasaki, M. Shinagawa, and K. Ochiai, "Principles and demonstration of intrabody communication with a sensitive electrooptic sensor," *IEEE Trans. Instrum. Meas.*, vol. 58, no. 2, pp. 457–466, Feb. 2009.

[11] M. S. Wegmueller, M. Oberle, N. Felber, N. Kuster, and W. Fichtner, "Signal transmission by galvanic coupling through the human body," *IEEE Trans. Instrum. Meas.*, vol. 59, no. 4, pp. 963–969, Apr. 2010.

[12] N. Haga, K. Saito, M. Takahashi, and K. Ito, "Proper derivation of equivalent-circuit expressions of intra-body communication channels using quasi-static field," *IEICE Trans. Commun.*, vol. E95, no. 1, pp. 51–59, Jan. 2012.
[13] M. A. Callejon, D. Naranjo-Hernandez, J. Reina-Tosina, and L. M. Roa, "Distributed circuit modeling of galvanic and capacitive coupling for intrabody communication," *IEEE Trans. Biomed. Eng.*, vol. 59, no. 11, pp. 3263–3269, Nov. 2012.
[14] Ž. Lučev, I. Krois, and M. Cifrek, "A capacitive intrabody communication channel from 100 kHz to 100 MHz," *IEEE Trans. Instrum. Meas.*, vol. 61, no. 12, pp. 3280–3289, Dec. 2012.
[15] M. Seyedi, B. Kibret, D. T. H. Lai, and M. Faulkner, "A survey on intrabody communications for body area network applications," *IEEE Trans. Biomed. Eng.*, vol. 60, no. 8, pp. 2067–2079, Aug. 2013.
[16] A. Sasaki, T. Ishihara, N. Shibata, R. Kawano, H. Morimura, and M. Shinagawa, "Signal-to-noise ratio analysis of a noisy-channel model for a capacitively coupled personal area network," *IEEE Trans. Antennas Propag.*, vol. 61, no. 1, pp. 390–402, Jan. 2013.
[17] A. Sasaki et al., "Extended noisy-channel models for capacitively coupled personal area network under influence of a wall," *IEEE Trans. Antennas Propag.*, vol. 62, no. 5, pp. 2802–2812, May 2014.
[18] J. Bae and H.-J. Yoo, "The effects of electrode configuration on body channel communication based on analysis of vertical and horizontal electric dipoles," *IEEE Trans. Microw. Theory Techn.*, vol. 63, no. 4, pp. 1409–1420, Apr. 2015.
[19] J. Park, H. Garudadri, and P. P. Mercier, "Channel modeling of miniaturized battery-powered capacitive human body communication systems," *IEEE Trans. Biomed. Eng.*, vol. 64, no. 2, pp. 452–462, Feb. 2017.
[20] J. Mao, H. Yang, Y. Lian, and B. Zhao, "A self-adaptive capacitive compensation technique for body channel communication," *IEEE Trans. Biomed. Circuits Syst.*, vol. 11, no. 5, pp. 1001–1012, Oct. 2017.
[21] V. Varga, G. Vakulya, A. Sample, and T. R. Gross, "Enabling interactive infrastructure with body channel communication," in *Proc. ACM Interact., Mobile, Wearable Ubiquitous Technol.*, vol. 1, no. 4, p. 169, Dec. 2017.
[22] D. Naranjo-Hernández, A. Callejón-Leblic, Ž. L. Vasi, M. Seyedi, and Y.-M. Gao, "Past results, present trends, and future challenges in intrabody communication," *Wireless Commun. Mobile Comput.*, vol. 2018, Mar. 2018, Art. no. 9026847.
[23] J. Zhao, J. Mao, T. Zhou, L. Lai, H. Yang, and B. Zhao, "An auto loss compensation system for non-contact capacitive coupled body channel communication," in *Proc. IEEE Int. Symp. Circuits Syst. (ISCAS)*, Florence, Italy, May 2018, pp. 1–5, doi: 10.1109/ISCAS.2018.8351340.
[24] V. Varga, M. Wyss, G. Vakulya, A. Sample, and T. R. Gross, "Designing groundless body channel communication systems: Performance and implications," in *Proc. 31st Annu. ACM Symp. User Interface Softw. Technol.*, Berlin, Germany, Oct. 2018, pp. 683–695.
[25] T. Hachisu, B. Bourreau, and K. Suzuki, "EnhancedTouchX: Smart bracelets for augmenting interpersonal touch interactions," in *Proc. CHI Conf. Hum. Factors Comput. Syst.*, Glasgow, U.K., May 2019, p. 321.
[26] W. J. Thomlinson, S. Banou, C. Yu, M. Stojanovic, and K. R. Chowdhury, "Comprehensive survey of galvanic coupling and alternative intra-body communication technologies," *IEEE Commun. Surveys Tuts.*, vol. 21, no. 2, pp. 1045–1164, 2nd Quart., 2019.
[27] S. Maity, M. He, M. Nath, D. Das, B. Chatterjee, and S. Sen, "Bio-physical modeling, characterization, and optimization of electro-quasistatic human body communication," *IEEE Trans. Biomed. Eng.*, vol. 66, no. 6, pp. 1791–1802, Jun. 2019.
[28] D. Das, S. Maity, B. Chatterjee, and S. Sen, "Enabling covert body area network using electro-quasistatic human body communication," *Sci. Rep.*, vol. 9, no. 1, p. 4160, Dec. 2019.
[29] W. J. Tomlinson, S. Banou, S. Blechinger-Slocum, C. Yu, and K. R. Chowdhury, "Body-guided galvanic coupling communication for secure biometric data," *IEEE Trans. Wireless Commun.*, vol. 18, no. 8, pp. 4143–4156, Aug. 2019.
[30] W. K. Chen et al., "Design of galvanic coupling intra-body communication transceiver using direct sequence spread spectrum technology," *IEEE Access*, vol. 8, pp. 84123–84133, 2020.
[31] I. Culjak, Ž. L. Vasic, H. Mihaldinec, and H. Džapo, "Wireless body sensor communication systems based on UWB and IBC technologies: State-of-the-art and open challenges," *Sensors*, vol. 20, no. 12, p. 3587, Jun. 2020.
[32] H.-Y. Shih, Y.-C. Chang, C.-W. Yang, and C.-C. Chen, "A low power and small chip-area multi-rate human body communication DPFSK transceiver for wearable devices," *IEEE Trans. Circuits. Syst., II, Exp. Briefs*, vol. 67, no. 7, pp. 1234–1238, Jul. 2020.
[33] M. B. Lodi et al., "A periodic transmission line model for body channel communication," *IEEE Access*, vol. 8, pp. 160099–160115, 2020.
[34] S. Maity, M. Nath, G. Bhattacharya, B. Chatterjee, and S. Sen, "On the safety of human body communication," *IEEE Trans. Biomed. Eng.*, vol. 67, no. 12, pp. 3392–3402, Dec. 2020.
[35] M. Nath, S. Maity, S. Avlani, S. Weigand, and S. Sen, "Inter-body coupling in electro-quasistatic human body communication: Theory and analysis of security and interface properties," *Sci. Rep.*, vol. 11, no. 1, p. 4378, 2021.
[36] D. C. Nguyen et al., "6G Internet of Things: A comprehensive survey," *IEEE Internet Things J.*, vol. 9, no. 1, pp. 359–383, Jan. 2022.
[37] A. Sasaki, K. Morita, and A. Ban, "Machine-learning approach for binary classification of signal transmission modes in human body communication channels," in *Proc. Int. Conf. Emerg. Technol. Commun. (ICETC)*, Dec. 2020, Art. no. B2-4.
[38] A. Sasaki and A. Ban, "Machine-learning approach to binary classification of uplink-channel states for secure body-coupled communication," in *Proc. Int. Conf. Emerg. Technol. Commun. (ICETC)*, Dec. 2021, Art. no. A1-1.
[39] C. M. Bishop, *Pattern Recognition and Machine Learning*. New York, NY, USA: Springer-Verlag, 2006.
[40] E. Alpaydin, *Introduction to Machine Learning*. Cambridge, MA, USA: MIT Press, 2010.
[41] M. Mohri, A. Rostamizadeh, and A. Talwalkar, *Foundations of Machine Learning*. Cambridge, MA, USA: MIT Press, 2012.
[42] K. P. Murphy, *Machine Learning: A Probabilistic Perspective*. Cambridge, MA, USA: MIT Press, 2012.

Ai-ichiro Sasaki (Member, IEEE) received the B.S. degree in applied physics from Tokyo University of Science, Tokyo, Japan, in 1996, the M.S. degree in physics from the University of Tokyo, Tokyo, in 1998, and the Ph.D. degree in electrical engineering from Tokyo University of Science in 2006.

From 1998 to 2018, he worked as a Researcher with the NTT Science and Core Technology Laboratory Group, Kanagawa, Japan. In 2018, he was appointed as an Associate Professor of the Department of Electronic Engineering and Computer Science, Kindai University, Hiroshima, Japan. His research interests include electromagnetic technologies ranging from the low-frequency band to optical wavelengths and their applications to intelligent sensing and communications.

Dr. Sasaki is a member of the Physical Society of Japan, the Japan Society of Applied physics, the Institute of Electrical Engineers of Japan, and the Institute of Electronics, Information, and Communication Engineers of Japan (IEICE). He served as an Editor for the *IEICE Electronics Express*.

Akinori Ban received the B.E. degree in electronic engineering and computer science from Kindai University, Hiroshima, Japan, in 2021, where he is currently pursuing the M.E. degree.

His research interests include wireless sensing and communication systems and machine learning.

Mr. Ban is a member of the Institute of Electronics, Information, and Communication Engineers of Japan (IEICE).